Nano Research

ISSN 1998-0124 CN 11-5974/O4
https://doi.org/10.1007/s12274-021-3607-5

Review Article

Mechanisms of water oxidation on heterogeneous catalyst surfaces

Xiaogang Yang[1,§] (✉), Yuanxing Wang[2,§], Chang Ming Li[1,3], and Dunwei Wang[2] (✉)

[1] *Institute of Materials Science and Devices, School of Materials Science and Engineering, Suzhou University of Science and Technology, Suzhou 215011, China*
[2] *Department of Chemistry, Boston College, Merkert Chemistry Center, MA 02467, USA*
[3] *Institute of Clean Energy & Advanced Materials, Southwest University, Chongqing 400715, China*
[§] *Xiaogang Yang and Yuanxing Wang contributed equally to this work.*

Received: 18 March 2021 / **Revised:** 6 May 2021 / **Accepted:** 19 May 2021

ABSTRACT

Water oxidation, an essential step in photosynthesis, has attracted intense research attention. Understanding the reaction pathways at the electrocatalyst/water interface is of great importance for the development of water oxidation catalysts. How the water is oxidized on the electrocatalyst surface by the positive charges is still an open question. This review summarizes current advances in studies on surface chemistry within the context of water oxidation, including the intermediates, reaction mechanisms, and their influences on the reaction kinetics. The Tafel analyses of some electrocatalysts and the rate-laws relative to charge consumption rates are also presented. Moreover, how the multiple charge transfer relies on the intermediate coverage and the accumulated charge numbers is outlined. Lastly, the intermediates and rate-determining steps on some water oxidation catalysts are discussed based on density functional theories.

KEYWORDS

water oxidation, intermediate, rate-determining step, rate-law, Tafel analysis, density functional theory

1 Introduction

Modern society relies on the vast energy consumption of fossil fuels, which cannot be sustained for long-term development without renewable energies. Natural photosynthesis (PS), one of the most important processes in the earth, captures a fraction of the energy (89 TW) from the total solar illumination to Earth (1.24×10^5 TW) [1]. Inspired by natural photosynthesis, artificial photosynthesis has been studied for over half-century because it holds great promises for substituting fossil fuels with clean energies [2]. The general scheme of artificial photosynthesis involves driving both the reduction and oxidation half-reactions either directly using solar energy through photocatalysis or photoelectrochemical (PEC) synthesis or indirectly using solar electricity through electrocatalysis [3]. The common chemistry is converting and storing electric/photon energy in chemical bonds as chemical energy [4–6]. For solar fuel production systems, the oxidation of water to molecular oxygen is a critical step (or half-reaction) as it provides a viable source of electrons for hydrogen generation or the reduction of carbon dioxide [7, 8]. For example, sluggish water oxidation is regarded as the bottleneck that limits the overall reaction rates, which attracts much research attention.

Indeed, a large number of catalysts have been investigated for water oxidation, and their performance has been significantly improved for potential future applications [9]. To be practically viable, not only the activity and efficiency, but also other technical parameters such as stability, scalability, and cost should be evaluated based on existing techno-economic analysis models [10]. Obviously, activity and efficiency are two important factors for any catalysts under consideration that are connected to the fundamental properties. In recognition that surface chemistry plays a critical role in determining the performance of a heterogeneous catalyst but has received insufficient attention in recent other reviews, we choose to focus our discussions in this article on this point.

Before going too far, we must recognize that water-splitting technologies are far from being economically competitive for practical solar fuel productions [10]. One of the main reasons that limit progress in this field is the big gap in understanding water oxidation mechanisms. The high performance of heterogeneous catalysts is often proposed to be originated from their unique structures [11]. The water oxidation on heterogeneous (photo)electrocatalyst is a unique three-phase chemical reaction system, which is strongly determined by the surface interaction between the water molecules and the interfaces. For example, the vacancy, point defects in bulk materials and surface, the exposed lattice facets, the bridge sites, terrace kinks, edge structures, and coordination, significantly influence the activity of the catalyst. Different from molecular water oxidation catalysts that are homogeneously dissolved in water, heterogeneous catalysts do not show abundant catalytic sites in a well-defined single crystalline surface or unique catalytic sites in a complex polycrystalline surface [12, 13]. Such ambiguities greatly increase the difficulties in proposing a clear reaction mechanism, the lack of which has been a key reason for the sluggish progress in finding catalysts that can contribute to practical artificial photosynthesis. The problem is further exacerbated for systems where charge separation and transfer are convoluted, such as a PEC system, where both thermodynamics and kinetics can be

Address correspondence to Xiaogang Yang, yangxg@usts.edu.cn; Dunwei Wang, dunwei.wang@bc.edu

highly sensitive to the facets under consideration [14]. Within this context, we put together this paper to provide insights on structure–property relationships of heterogeneous catalysts for water oxidation. It is noted that there have been some excellent reviews on the topic of water oxidation. They focus on, for example, materials [4, 9], theoretical design [15, 16], and overviews of the field [13, 17]. Instead of replicating these efforts, we aim to center our discussions round the chemical mechanisms by which water is oxidized. We start from a brief introduction of water oxidation in natural photosynthesis and move on to examine the chemistry of heterogeneous catalyst-based water oxidation, including surface reaction pathways, intermediates involved, reaction mechanisms, kinetics as studied by techniques such as Tafel analyses and rate-law models, as well as theoretical density functional theory (DFT) calculations. Our ultimate goal is to reveal the relationship between the reaction process and the intermediates.

2 Learn from natural photosynthesis

Both natural and artificial water oxidation share the same chemical natures in neutral or acidic conditions: $2H_2O \rightarrow 4H^+ + O_2 + 4e^-$. Despite the efforts on artificial photosynthesis, the lack of suitable water oxidation catalyst is generally regarded as a bottleneck for practical industrial applications. Over three billion years of natural evolution, an identical chlorophyll (Chl) has been chosen and conserved in diverse species (plants, algae, and cyanobacteria) [18]. The miracle of natural photosynthesis is to drive carbohydrate production by abundant solar energy based on the chloroplasts and Mn_4CaO_5 catalytic cluster, which has efficient light absorption, charge separation, and charge transfer kinetics [19]. This Mn_4CaO_5 core catalyzes water oxidation to O_2 with a maximal turnover frequency of ~ 500 s^{-1} and a high turnover number of 10^6 [20], leaving much for scientists to learn in the quest of designing new catalysts.

The inorganic core in Chl has been well characterized by X-ray diffraction (XRD) from the protein complex in its dark-stable state $Mn_4CaO_5(H_2O)_4$. Umena et al., for instance, provided the high-resolution structure of the PSII crystals at 1.9 Å (Fig. 1(a)) [21]. The oxygen evolution reaction (OER) in natural photosynthesis was initially proposed as the S-state cycle of period-four oscillation with flash-induced photolysis by Bessel Kok in 1970 [22], which was further developed with the fine crystallographic PSII structure in 2001 [23]. It is now known that there are five oxidation states (S states) in the PSII catalytic cycle, in which four of them (S_0, S_1, S_2, and S_3) are stable with a relatively long lifetime of up to several seconds, whereas the lifetime of S_4 intermediate is short [24]. The S state of the Kok cycle can be verified in buffer solutions, as O_2 is only formed in the section of the $S_3 \rightarrow S_0$ transition [25]. Recently, the PSII crystal displayed several cycles of oxygen evolution with increased activity by the use of electron acceptors (e.g., quinone derivative or ferricyanide) [26], which further confirmed a four-step catalytic cycle of PSII.

Although more details about the water oxidation mechanisms at the inorganic Mn_4CaO_5 core remain a topic of debates, its fundamental importance to understanding how the catalytic cycle of the S states takes place for both artificial and natural water oxidation systems is well recognized and agreed upon. In the S-cycle model, four successive light flashes are required for the O_2 generation. According to the femtosecond X-ray study by Kern et al. (Fig. 1(b)) [19], the light flash triggered charge transfer starting from the dark stable S_1 intermediate ($Mn_4(III_2,IV_2)$) to the S_2 state ($Mn_4(III,IV_3)$) by storing one positive charge. In the transition of $S_2 \rightarrow S_3$ with the second light stroke, a second Mn is oxidized from 3^+ to 4^+, forming the S_3 ($Mn_4(IV_4)$) state. The elusive S_4 state is a transiently formed intermediate in the $S_3 \rightarrow S_0$ transition, which is particularly important for the O–O bond formation. After the release of another proton and an oxygen molecule, it returns back to the S_0 state ($Mn_4(III_3,IV)$). The findings during the oxygen evolution demonstrate some key information: Natural OER relies on the positive charges stored in multiple metal sites; the reaction takes place through a four-charge-transfer process; existing mechanistic studies benefit from the existence of long-lived intermediates and the structural information of intermediates in angstrom scale.

3 Artificial water oxidation mechanisms

Water oxidation reactions are considered to take place following a similar process on electrocatalysts, photocatalysts, and photoelectrocatalysts. The difference mainly lies in how the charges are generated. For instance, a bias is required for electrocatalysts, whereas photons are required for photocatalysts, and photoelectrocatalysts need both. What's in common is the chemical reaction between water molecules and the positive charges on the catalyst surfaces. First, water oxidation on heterogeneous catalysts can take place for at least three products, to form OH radicals [27], H_2O_2 [28], or O_2. The radical and hydrogen peroxide formation is usually more difficult due to the higher free energy increase associated with the change. Moreover, the radical or peroxide products are less stable [29], so that the OER is more general to be desired for many water oxidation reactions.

The sluggish part of the water-splitting reaction is the OER,

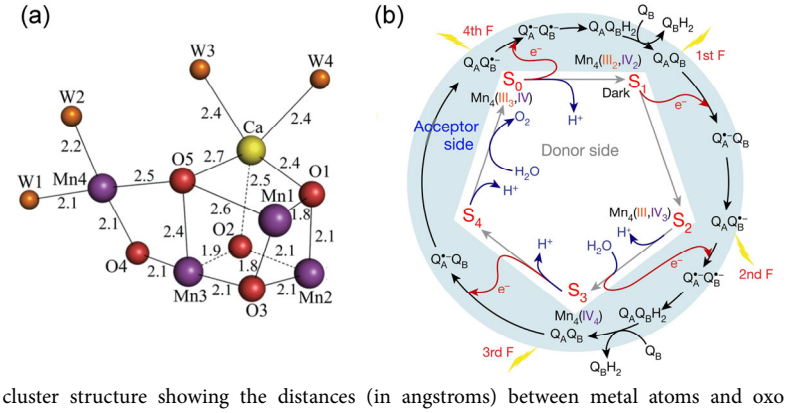

Figure 1 (a) The Mn_4CaO_5 cluster structure showing the distances (in angstroms) between metal atoms and oxo bridges or water molecules. Reproduced with permission from Ref. [21], © Macmillan Publishers Limited 2011. (b) The oxygen-evolving cycle in photosystem II, showing the relationship between the redox chemistry at the donor (Kok's clock) and acceptor sides throughout the oxygen-evolving cycle. Reproduced with permission from Ref. [19], © Springer Nature Limited 2018.

which is the half-reaction occurring at the anode parts (Eq. (1), E_a° =1.23 V vs. the normal hydrogen electrode) [17]

$$2H_2O_{(l)} \longrightarrow O_{2(g)} + 4H^+ + 4e^- \quad (1)$$

By comparison, hydrogen evolution reaction (HER) on the cathode generally shows much faster reaction kinetics as manifested by a smaller overpotential. Inspired by the mechanisms proposed for natural PS, OER is typically understood to proceed through four elementary steps, providing four protons and four electrons with the release of one molecular O_2. The four-electron-transfer process in OER increases the complexity of electrolysis and accounts for the large energy loss in OER.

Among many proposed mechanisms, there are two primary ones for the OER: water nucleophilic attack (WNA) and interaction of two metal-oxo entities (I2M) (Fig. 2(a)) [30]. For WNA, as one of the simplest models, it is proposed to work through proton-coupled electron (or hole) transfers (PCET) between four intermediates (* → *OH → *O → *OOH → *, * stands for an active site) on a single catalytic site in a turnover (Eqs. (2)–(5)).

$$H_2O + * \longrightarrow *OH + H^+ + e^- \quad (2)$$

$$*OH \longrightarrow *O + H^+ + e^- \quad (3)$$

$$H_2O + *O \longrightarrow *OOH + H^+ + e^- \quad (4)$$

$$*OOH \longrightarrow O_2 + H^+ + e^- + * \quad (5)$$

Both WNA and I2M paths start with PCET steps including the same intermediates such as M–OH and M=O, while the major difference is the formation of an O–O bond. Suen et al. have reviewed possible OER mechanisms by two classical procedures through the oxygen formation from the peroxide terminal path and the oxo coupling path, respectively [17]. Regarding the WNA mechanism, a M=O species proceeds to form an O–O bond through the nucleophilic attack of a water molecule and a PCET step. For the I2M mechanism, the formation of an O–O bond involves the coupling of two neighboring M=O species, which is also named as intramolecular oxygen coupling (IMOC) mechanism [31]. In addition to proceeding on metal atoms based on conventional catalytic considerations, researchers have also suggested that the reaction may take place on the lattice oxygen sites [32], which is termed as lattice oxygen activation mechanism (LOM) or lattice oxygen evolution reaction (LOER). Recently, by using *in situ* mass spectrometry, Shao-Horn et al. [33] and Cherevko et al. [34] provided direct experimental evidence that lattice oxygen in some active oxides indeed participates in the generation of O_2 during the OER, respectively. This lattice participation mechanism (Fig. 2(b)) is different from the traditional WNA or I2M mechanisms and brings new insights for the understanding of OER because it does not rely on the formation of M–OH. This consideration invokes surface vacancy (□) as yet another type of intermediates that may form multiple coordinates with lattice metal atoms. Huang et al., for example, found that OER could take place through the LOM mechanism on zinc-substituted CoOOH catalysts [35] when the frontier orbitals of two neighbouring oxidized oxygen atoms hybridize without significantly sacrificing metal-oxygen hybridization. Pan et al. prepared Si-doped strontium cobaltite ($SrCoO_3$) [36] and observed that OER can be enhanced by improved oxygen diffusivity. It is also noted that non-metal atoms may also serve as the catalytic sites [37, 38].

Generally speaking, the WNA, I2M, and LOER processes may be identified by the catalysts on which the O–O bond is formed. For WNA, the O–O bond is formed between an electrophilic *O and a nucleophilic water molecule on a single catalytic site. For the I2M process, the O–O bond is formed between two *O units with radical characteristics on two adjacent sites [39]. For the lattice participation mechanism, the oxygen in the reactive species may interface/exchange with lattice oxygen [35]. For all mechanisms discussed here, the intermediates are generally regarded as a key piece of evidence that needs to be experimentally verified.

4 Elusive intermediates detection

The validation of intermediates during the reaction offers critical information on the proposed mechanism [40]. Water oxidation on a heterogeneous surface involves bond formation/rupture and lattice atoms through multiple steps. Most proposed mechanisms share the same intermediates, such as *, *OH, *O, *OOH (* denotes as the active site at the heterogenous catalyst as described above), which can be formed either on metal, non-metal centers, or lattice vacancies. It is well known that the surface of metal oxides can be partially covered with molecular H_2O or hydroxyl groups, which are likely involved in the surface reaction kinetics when the electrode is contacted with water in the electrolyte, under applied bias or exposed to photon irradiation.

Surface intermediates are sensitive to interactions between water species and catalyst materials. For example, the chemical adsorption of water is stable up to 256 and 356 °C on anatase and rutile TiO_2, respectively [41]. According to the calculated *OH formation energy, water is preferred to be adsorbed dissociatively as *OH on rutile (110) [42] and anatase (001), while non-dissociatively adsorbed on anatase (101) surface [43]. Differently, the surface of hematite is relatively stable, showing primarily oxygen termination (*O) and molecular water covered on (001) [44]. This observation has been attributed to the larger formation energy of *OH ($\Delta G_{OH} - \Delta G_*$) on hematite. WO_3 is even more inert so that H_2O is preferably adsorbed in an undissociated molecular form on the (001) surface with primarily *O termination rather than *OH [45, 46].

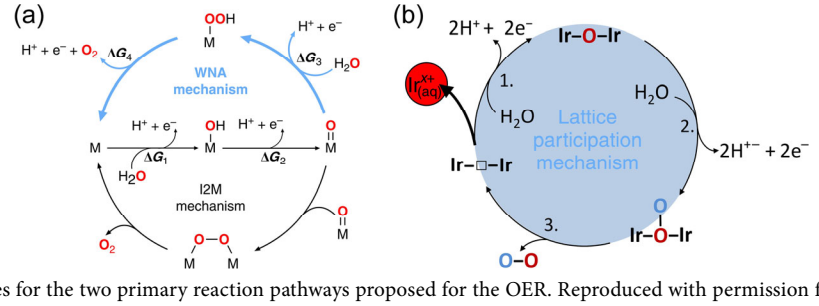

Figure 2 (a) Catalytic cycles for the two primary reaction pathways proposed for the OER. Reproduced with permission from Ref. [30], © Craig, M. J. et al. 2019. (b) The mechanism suggested for amorphous iridium oxide and leached perovskites with the participation of activated oxygen in the reaction forming oxygen vacancies. Adapted with permission from Ref. [34], © Macmillan Publishers Limited, part of Springer Nature 2018.

For $BiVO_4$, it is revealed that water is adsorbed molecularly on the Bi site, according to first-principle molecular dynamic calculations [47]. The higher formation energy for *OH revealed dissociative water adsorption was more difficult [48]. By contrast, surface Fe(II) species enable the formation of surface *OH species. Ambient-pressure X-ray photoelectron spectroscopy experiments revealed that *OH can exist at the interface on a vacuum-prepared α-Fe_2O_3(0001) surface [44]. Oxygen vacancies can decrease *OH formation energy, which facilitates dissociative adsorption on h-WO_3(100) and forms *OH on the surface [49].

As discussed above, the O–O bond formation is regarded as a key piece of evidence for mechanistic studies. Thus, the detection of O–O related intermediates is critically important. However, due to the high formation energy (or fast depletion rate) of *OOH, the observation of this functional group has been elusive. More broadly, to validate a reaction mechanism, it should be helpful to monitor other intermediates, including *OH, *O, and even empty sites, as well.

Fourier transform infrared (FT-IR) spectroscopy, a structure-specific technique, is suitable for detecting these surface intermediates and recording time-dependent behaviors [40]. To confirm a proposed mechanism and identify active intermediates for a reaction, *in situ* experiments are commonly conducted to provide valuable and vital information since such conditions can most accurately replicate what happens under realistic reaction conditions. Nevertheless, few *operando* experiments have been reported for the study of immobilized electrocatalysts at the solid/liquid interface. For water oxidation, researchers often use the attenuated total reflection (ATR) technique to minimize the strong IR absorption of H_2O in the liquid phase [50]. By rapid-scan ATR-FTIR spectroscopy (Fig. 3(a)), for instance, Frei et al. detected a surface hydroperoxide intermediate (830 cm^{-1}, Fig. 3(b)) on Ir oxide nanoclusters under pulsed visible excitation of a $[Ru(bpy)_3]^{2+}$ sensitizer for water oxidation [50]. With the help of isotope ^{18}O labelling, they identified the surface intermediate as an Ir-OOH species. Based on this result, they proposed a partial mechanism for water oxidation on Ir oxide surface that the O–O bond was formed by the reaction of an Ir^{v}=O with the attack of H_2O. In follow-up work, they achieved time-resolved detection of water oxidation intermediates on cobalt oxide nanoparticles using a similar experimental configuration [51]. One intermediate was surface superoxide (1,013 cm^{-1}, Fig. 3(c)), and another intermediate was a Co^{v}=O site (840 cm^{-1}, Fig. 3(d)). The different time-dependent behaviors of these intermediates indicated that they were associated with different catalytic sites. The superoxide intermediate grew on catalytically fast sites as O_2 evolved with photolysis pulses, whereas the Co^{v}=O group were generated on catalytically slow sites.

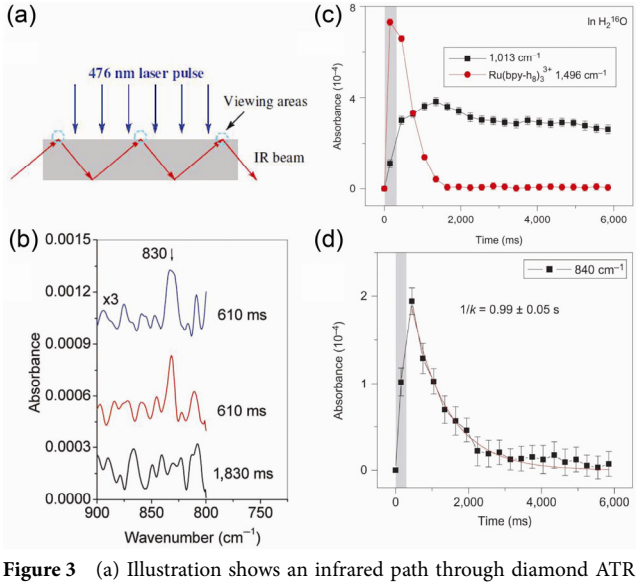

Figure 3 (a) Illustration shows an infrared path through diamond ATR element. (b) Rapid-scan FT-IR traces in the 900–700 cm^{-1} region: 610 ms (light on) and 1,830 ms spectra (light off) for the photo-oxidation of H_2O. (a) and (b) are reproduced with permission from Ref. [50], © American Chemical Society 2011. (c) The infrared bands of superoxide intermediate (1,013 cm^{-1}) and oxidized sensitizer $Ru(bpy\text{-}h_8)_3^{3+}$ (1,496 cm^{-1}) on visible light-sensitized water oxidation at Co_3O_4 catalyst in $H_2{}^{16}O$. (d) The decay following a 476 nm laser pulse is shown for Co_3O_4 catalyst in $H_2{}^{16}O$. (c) and (d) are reproduced with permission from Ref. [51], © Macmillan Publishers Limited 2014.

Combined with electrochemical measurements, *operando* ATR-FTIR spectroscopy can also identify surface intermediates under PEC water oxidation conditions (Fig. 4(a)) [52]. By using an ATR-FTIR setup, Hamann et al. detected a PEC water oxidation intermediate on hematite surfaces [52]. The Fe–oxo group displayed an IR vibration absorption with frequency in the range of 750–900 cm^{-1}. Moreover, the absorption peak at 898 cm^{-1} appeared at the onset potential above 1.7 V under dark or 1.25 V under illumination vs. the reversible hydrogen electrode (RHE), where the IR signal corresponded to the current built up for water-oxidation. This potential- and light-dependent absorption peak was identified as a Fe^{IV}=O species (898 cm^{-1}, Fig. 4(b)). Based on this finding, the authors established a PEC water oxidation mechanism (similar to Eqs. (2)–(5)) on hematite that a Fe=O species was formed as the first oxidized product by valence-band holes. Subsequent attack by a H_2O molecule could produce a peroxide intermediate on the surface that generates oxygen during the following steps [52]. Using similar *operando* ATR-FTIR spectroscopy, Zhao et al. investigated O–O bond formation pathways for PEC water oxidation on hematite photoanode in less basic electrolytes [39]. They identified a potential-dependent vibration band to a superoxide group (1,100 cm^{-1}, Fig. 4(c)). By adjusting the pH of the electrolyte, the authors observed that this IR band was most prominent at pH 8. Its intensity decreased with increased

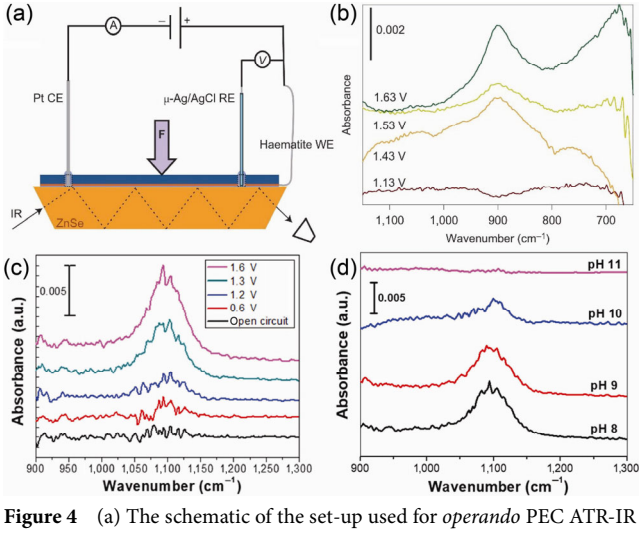

Figure 4 (a) The schematic of the set-up used for *operando* PEC ATR-IR measurements. (b) Infrared spectra of hematite at constantly applied potentials from 1.13 to 1.63 V vs. RHE, under illumination. (a) and (b) are reproduced with permission from Ref. [52], © Macmillan Publishers Limited 2016. (c) FT-IR spectra on the hematite photoanode under illumination in unbuffered pH 8 electrolyte at 0.6–1.6 V vs. RHE. (d) FT-IR spectra on the hematite photoanode under illumination with an applied potential of 1.6 V vs. RHE at different pHs. (c) and (d) are reproduced with permission from Ref. [39], © American Chemical Society 2018.

pH and vanished at pH 11 (Fig. 4(d)). The IR frequency of superoxide group formation is consistent with the scattering peaks (800–1,350 cm^{-1}) on NiOOH by surface-enhanced Raman spectroscopy [53]. The pH-dependent IR absorption indicated that the observed superoxide only accumulated under near-neutral conditions, where the surface hole transfer happened through the WNA mechanism [39]. Recently, we applied surface-enhanced infrared absorption spectroscopy in the ATR geometry for monitoring the O–O bond intermediates formation on $CoO_x(OH)_y$ electrocatalyst during water oxidation, where it can be used to identify whether the water molecules are involved in WNA or I2M (IMOC) process [54]. All aforementioned works demonstrated that the understandings of the structure and kinetics of intermediates provide critical information on the identification of the water oxidation mechanisms, promoting the design of efficient water oxidation catalysts [40, 51].

Besides FT-IR, transient absorption spectroscopy in the ultraviolet–visible region also shows a correlation to PEC signals. The various absorption features can be assigned to band absorption due to electrons or holes [55], as well as positive equivalents (e.g., Fe=O). For instance, the absorption band attributed to Mn^{3+} at 510 nm was observed on δ-MnO_2 films at its onset potential [7]. The transient absorption of anatase TiO_2 photoanode showed visible absorption at various applied potentials [56], corresponding to hole absorption in TiO_2.

5 Reaction kinetics as studied by Tafel analysis

Based on the identification of the intermediates and the understanding of possible reaction mechanisms, one may ask critical questions such as, "what is the fundamental limitation for water oxidation?" and "how to increase the intrinsic reaction kinetics of water oxidation?" Practically, one may increase the applied voltage between the electrodes to accelerate the water oxidation rate on the electrocatalyst. The Tafel equation can be used to describe the relationship between the applied overpotential and the current density [57, 58]. Under this condition, the mass transfer of all other steps, such as the charge mobility, water, ions, and gas diffusion is assumed fast enough, so that only the electrochemical potential affects the electrochemical reaction rate. Thus, the current can be expressed as follows

$$\eta = a + b\log i \tag{6}$$

where $b = \dfrac{2.303RT}{\alpha nF}$ is the Tafel slope, i is the current density, n is the number of transferred charges in the reaction, F is the Faradaic constant, η is overpotential, α is the transfer coefficient, R is gas constant, and T is temperature.

The Tafel slope b represents how the current changes with the overpotential. For the ideal transfer coefficient (e.g., α is 0.5 for metal) and single electron transfer reactions, the Tafel slope is 120 mV·dec^{-1}. For multiple charge transfer reactions, a smaller Tafel slope could be observed, indicating that current densities increase faster with a smaller increased overpotential. Since most electrochemical reactions involve multiple-electron transfers, the Tafel slope can be deduced from microkinetic calculations that the number of electrons transferred before the rate-determining step (RDS) should also contribute. According to an early study [58], when the RDS involves a single-electron transfer process, the Tafel slope of the overall reaction could be 120 or 40 mV·dec^{-1}. When the RDS involves a non-electron transfer process, the Tafel slopes will be 60 or 30 mV·dec^{-1}. However, the ambiguity is the difficulty in the confirmation of the RDS and intermediates on other materials, where the initial state may not be 100% covered by * site (on RuO_2). Thus, the importance of understanding surface intermediates becomes clear.

The electrochemical reaction kinetics is sensitive to the nature of the intermediates, as the intermediate coverage varies with the applied potential. In the comprehensive Tafel slope calculation reported by Shinagawa et al. [57], they elucidated how the Tafel slopes were influenced by the surface intermediate coverage, and even the RDS of the whole reaction was the same. In their simple multiple-step (5-step, Eqs. (7)–(11)) reaction model, four intermediates such as *, *OH, *O, and *OOH on the surface as an electrocatalytic site for the OER cycle were studied in an alkaline solution. The RDS in the first step would limit all the following reaction steps so that the Tafel slope of the whole reaction will be 120 mV·dec^{-1} just like a single-electron transfer reaction. For example, when the *OH formation is the RDS in Eq. (7), and the surface intermediate is highly covered by empty site *, or when the *OOH formation is the RDS (in Eq. (9)) and the surface intermediate is dominated by *O, a slope > 120 mV·dec^{-1} will be detected.

$$OH^- + * \longrightarrow *OH + e^- \tag{7}$$

$$OH^- + *OH \longrightarrow *O + H_2O + e^- \tag{8}$$

$$*O + OH^- \longrightarrow *OOH + e^- \tag{9}$$

$$*OOH + OH^- \longrightarrow *OO^- + H_2O \tag{10}$$

$$*OO^- \longrightarrow * + O_2 + e^- \tag{11}$$

Recently, Liu et al. further addressed the issue connected to intermediate coverage. The surface intermediate coverage varies with the formation energy of intermediate and applied potential (in Fig. 5(a)) under steady-state conditions [59]. A three-dimensional (3D) plot of intermediate coverage shows each of the changes of intermediates with the applied potential and the catalyst adsorption. Even the RDS is in the first *OH formation step (with the ΔG_{OH} below 2.2 eV), the surface can be covered partially by *OH termination at high applied potentials.

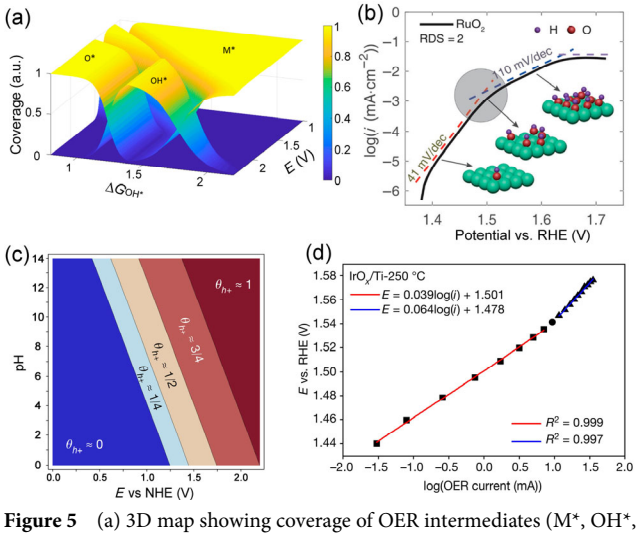

Figure 5 (a) 3D map showing coverage of OER intermediates (M*, OH*, and O*) vs. applied potentials and OH* adsorption energies. (b) Tafel plots of the as-synthesized RuO_2. The inset shows a schematic illustration of the change in surface coverage of OH* with an increase in overpotential. (a) and (b) are adapted with permission from Ref. [59], © American Chemical Society 2020. (c) Computed surface pH–potential phase diagram of hole coverage for a rutile-type IrO_2 (110) surface. (d) Measured Tafel plot from pulse voltammetry of IrO_x/Ti-250 °C. (c) and (d) are adapted with permission from Ref. [60], © Nong, H. N. et al. 2020.

In Fig. 5(b), assuming the RDS was in the second step (e.g., *O formation), they showed a Tafel slope of 110 mV·dec^{-1} on RuO_2 [59]. It is worth mentioning that the Tafel slope decreased once the RDS was closer to the end step of a series of steps. In addition, the surface intermediates could switch from empty sites to *OH-terminated sites with increased overpotentials. In Fig. 5(b) [59], the Tafel slope changed due to changed intermediate coverage (*OH domination) with the overpotential during the electrochemical measurements, and the measured Tafel slope was 41 mV·dec^{-1} for RuO_2 around the onset of OER.

Except for surface intermediate coverage, surface charge density also affects the Tafel slope. According to a recent capacitive charge storage study on IrO_x, Nong et al. [60] have demonstrated the charge storage influence on the OER rate by DFT calculations. The theoretical equilibration of IrO_2 (110) surfaces in water showed that the surface hole density (θ_{h+}) is dependent on both the potential and pH (Fig. 5(c)). The calculated Tafel plots are in good agreement with experimental results on crystalline IrO_2, where the experimental Tafel plot shows the Tafel slope of 39 mV·dec^{-1} below 1.54 V and 64 mV·dec^{-1} above 1.54 V (Fig. 5(d)). The change in the Tafel slope can be ascribed to a change in surface hole coverage under the applied potential (diagram in Fig. 5(c)) rather than to the surface intermediates coverage change [57]. The kinetics and Tafel analyses of those (photo)electrocatalysts provide information, such as how the charges are transferred through the interface between the electrocatalyst and the electrolyte.

It is noted that for a reaction with the same intermediate formation as RDS, different Tafel slopes could be obtained at low or high overpotentials. On the other hand, reactions with different RDS steps and consecutive reaction steps may display the same Tafel slope. Therefore, the choice for a suitable reaction mechanism should be based on collective examinations more than the Tafel analysis alone.

6 Rate-law studies

The reaction kinetics on electrocatalysts has been studied by more than Tafel analysis. Fundamentally, the reaction kinetics of water oxidation depends on how the reactants (water or hydroxyl anions, positive charges) are consumed at the solid/electrolyte interface. In the electrolysis, the positive overpotential is applied at the solid/electrolyte interface to modulate the anodic current, where the potential mainly drops in the Helmholtz layer for the metal electrocatalysts. However, for less conductive electrocatalysts or photoelectrocatalysts, the potential drop in the Helmholtz layer strongly depends on both the applied potential and carrier density. Therefore, it is important to monitor how the positive charge density influences the reaction kinetics. In principle, the rate-law of the water oxidation can be written as follows

$$J = k'_{WO} \cdot \left(h^+\right)^{\beta} \cdot [H_2O]^{\gamma} \quad (12)$$

where J and k'_{WO} are the current density (reaction rate) and rate-constant, respectively, and the hole density (h^+) and water concentration [H_2O] (supposing the reactant is H_2O; if OH^- is the reactant, the system can be treated accordingly) are considered; β and γ correspond to the reaction order of the reactant holes and water, respectively. It is well known that water in the electrolyte is in a large concentration that changes very little during the reaction, and the concentration of H_2O could be treated as a constant (when the activity of H_2O was alternated in the water-in-salt system [54], the reaction mechanism could be too much complicated to clarify). Thus, a simpler one could be shown

$$J = k_{WO} \cdot \left(h^+\right)^{\beta} \quad (13)$$

With the above equation, Durrant's group initiated the rate-law study of chemical reaction at the electrode interface to investigate how the reactants (e.g., the charge) contribute to the reaction kinetics. It can be converted to the following equation

$$\log J = \log k_{WO} + \beta \log\left(h^+\right) \quad (14)$$

By using this rate-law expression, one may predict the reaction mechanism based on information on how masses, such as charge, water molecules, and ions, are involved in the surface chemical reactions. However, there are relatively few experimental works focusing on the reaction order studies. Peter et al. developed photoelectrochemical impedance spectroscopy (PEIS) and intensity-modulated photocurrent spectroscopy (IMPS) techniques [61], where a 1st-order reaction was proposed in many PEC systems, including some water oxidation systems. In recent years, Durrant et al. employed photoinduced absorption spectroscopy coupled with transient photocurrent techniques on oxide surface during PEC reactions, to monitor the reaction kinetics of surface holes (may be intermediates or equivalents) [56, 62–64]. Zhao and his coauthors applied PEIS and *operando* FT-IR spectroscopy to probe the surface holes on hematite under steady-state illumination conditions [39].

For water oxidation, all the reaction orders from the 1st to 4th ones have been reported, indicating all scenarios of charge consumption are possible. For example, the most reported reaction order is 1st, which implies a single charge transfer process is the RDS of the overall reaction. Durrant et al. showed that both α-Fe_2O_3 [62] and $BiVO_4$ [63] photoanodes displayed first-order reaction kinetics at lower surface hole densities (e.g. < 1/nm^2). They found that the 1st-order kinetics was consistent with the measured charge lifetimes. The first-order behavior was explained by the hypothesis that a single surface hole is required to overcome the RDS in water oxidation at low surface hole densities. In a different group, Zhao and co-authors [39] observed a 1st order reaction at pH 8.0–10.0 on hematite when the charge density is lower than 0.8 hole/nm^2 (Fig. 6(a)). The reaction is supposed to occur through nucleophilic attack of a water molecule to form O–O bond (WNA mechanism), according to the successful detection of stretching vibration at 1,100 cm^{-1} from the intermediate (*-OOH) in Fig. 4(c).

For reaction order higher than 1, it indicates the reaction involves multiple charges consumed in a single elemental reaction step or in a multiple-step process in a single cycle. In Durrant's work on anatase, a second-order reaction was observed on TiO_2 with respect to holes in acidic and neutral conditions (Fig. 6(b)) [56]. They concluded that water oxidation on TiO_2 required multiple holes (or oxidized equivalents) to accumulate and overcome the RDS. The pH effect was also observed on hematite. A reaction order of 2.4 on hematite was obtained by Zhao et al. (Fig. 6(a)), when testing in alkaline $NaClO_4$ electrolyte (pH 13.6) [39]. They interpreted that the rate-limiting formation of O–O bond occurred through two *O coupling at neighbouring surface trapped holes.

Durrant et al. were among the first to observe 3rd order water oxidation reaction kinetics on hematite [62], anatase TiO_2 [56], and $BiVO_4$ [63] photoanode in the presence of a high hole density (Fig. 6(c)). Patzke's group recently observed the 3rd-order reaction kinetics on hematite photoanode in the presence of two surface states at 0.9 and 1.3 V, respectively, which was later interpreted as that the O–O formation was the RDS [65]. In their other two works on hematite, they observed

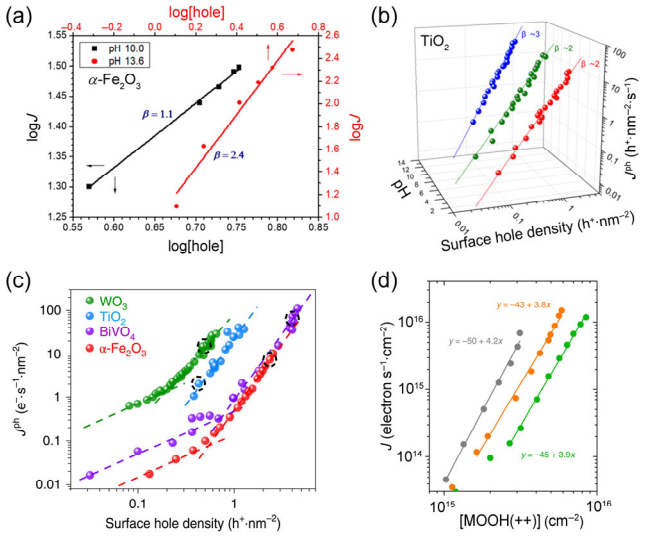

Figure 6 (a) Relationship of photocurrent densities and surface hole densities of pH 10.0 and pH 13.6 under illumination at 1.23 V vs. RHE. Reprinted with permission from Ref. [39], © American Chemical Society 2018. (b) Photocurrent vs. surface hole density and pH on TiO_2 at steady-state conditions during the oxidation of water (at 1.5 V vs. RHE). Reprinted with permission from Ref. [56], © American Chemical Society 2017. (c) Reaction rate vs. surface hole density for the α-Fe_2O_3 (β = 1, β = 3), TiO_2 (β = 3), WO_3 (β = 1, β = 2.5) and $BiVO_4$ (β = 1, β = 3). Reprinted with permission from Ref. [64], © Mesa, C. A. et al. 2019. (d) Rate law plots of the water oxidation current density vs. the concentration of MOOH(++) states for FeOOH (orange), Ni(Fe)OOH, and FeOOHNiOOH (green). Reprinted with permission from Ref. [68], © Francàs, L. et al. 2019.

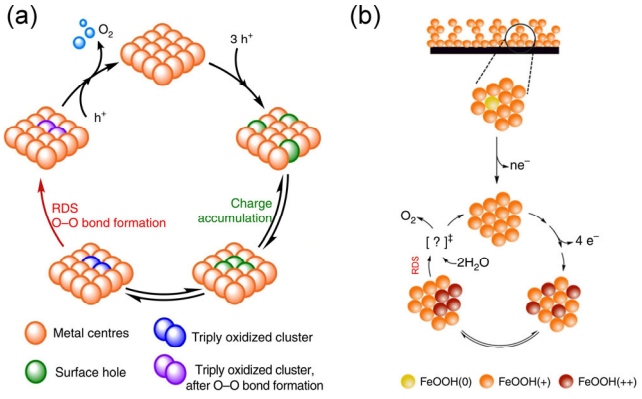

Figure 7 Mechanistic insights on water oxidation: (a) schematic of the key steps in the proposed third-order water oxidation reaction. Equilibration between three surface holes and M(OH)–O–M(OH) sites is followed by O–O bond formation as the RDS, which is followed by fourth oxidation and O_2 release. Adapted with permission from Ref. [64], © Mesa, C. A. et al. 2019. (b) Simple schematic representations of the water oxidation process based on the experimental observations for FeOOH. Adapted with permission from Ref. [68], © Francàs, L. et al. 2019.

2nd order kinetics on bare hematite nanorods array [66] but 3rd order kinetics on mesocrystal-based hematite photoanode [67]. For the 4th-order reaction, it is only reported on Ni/Fe oxyhydroxide films (Fig. 6(d)) [68]. Ni(Fe)OOH, FeOOH, and NiOOH electrocatalysts all exhibited a reaction order of approximately four when the current density ranged from 20 μA·cm^{-2}–1 mA·cm^{-2}. By rate-law analysis, Durrant et al. suggested that the RDS for each catalyst involves the accumulation of corresponding oxidized states: three holes for 3rd-order one and four holes for 4th-order one, respectively.

However, these reports did present discrepancies concerning certain materials (e.g., hematite) that can enable 1st, 2nd, and 3rd order reactions within the context of water oxidation. Cautions must be taken in interpreting the data. For instance, charge transport limitation (such as the diffusion distance) and charge densities, as well as pH, can all influence the measurements. It is well known that surface chemical intermediates will change with pH, potential, and photon irradiation intensity. Surface coverage may be another important factor that alters the reaction mechanisms. With these caveats noted, we emphasize that kinetic studies of water oxidation will likely play an important role in elucidating the reaction mechanisms on heterogeneous catalysts.

As discussed above, kinetic studies of water oxidation catalysts showed that the reaction is sensitive to charge densities. Based on calculations, high-reaction order can be attributed to multiple-charge accumulation. As an example, it is shown in Fig. 7(a) that the surface holes are assembled and equilibrated with triply oxidized equivalents for the RDS [64]. If starting from empty sites, three holes are used to convert surface positive equivalents (in green), which are discrete on the surface. Next, photogenerated holes accumulate near the catalytic sites through lateral diffusion, until the charges convert to form an oxidized cluster with triply oxidized charges (in blue) and enable O–O bond formation (in purple). The following step results in the dimer (O=^{IV}Fe–O–Fe^{IV}=O) formation by oxidation of the second Fe^{III}–OH, which corresponds to two neighbouring holes on the hematite surface. To overcome the RDS, additional holes are required to form the O–O bond. In the end, the 4th hole facilitates the O_2 release and enables another H_2O binding to the active site. The authors presented that water oxidation on hematite through the stepwise oxidations reminded us of how the Mn_4CaO_5 cluster in natural PS works: The reaction requires multiple oxidized equivalents that can aggregate on different sites. The O–O bond formation can be detected on hematite photoanode by Hamann's method [52]. While for Fe=O intermediates, it has been detected by the transient absorption spectroscopy as surface holes. Figure 7(b) depicts a simple mechanistic scheme for the 4th-order reaction on Ni(Fe)OOH electrocatalyst. As shown above, Durrant et al. found that FeOOH, Ni(Fe)OOH, and FeOOH/NiOOH could display fourth-order kinetics [68]. Although directly probing reactive intermediates during water oxidation is extremely difficult, spectroelectrochemical characterization showed the concentration of oxidized species. Without separately investigating short-lived reactive intermediates, they proposed that four oxidized species were required to overcome the RDS.

7 Prediction by density functional theories

As shown above, the reaction kinetics can be experimentally studied through the Tafel method and rate-law analyses, where both techniques help to reveal correlations of the experimental observations with the RDS and surface intermediates. However, the conclusions are usually speculative with significant uncertainties. Moreover, the reaction model as shown in Eqs. (13) and (14) is still highly rudimentary, thus no definitive relationship can be easily established yet. To better understand the catalytic process and identify the promising candidate materials or structures, first-principle calculations, for example, DFT can be developed to deal with ideal single crystalline surface and can be applied to calculate the energy levels of various intermediates [69].

One typical approach is widely applied using the four intermediates through a four-step charge transfer reaction (Eqs. (2)–(5)). In a pioneering work, DFT predictions have been developed by Valdés and Nørskov [70–72], where numerous theoretical predictions of water oxidation have been carried out on various metal oxides [73, 74]. The energy barrier between

each intermediate state was the free energy increase (ΔG_n), which can be roughly regarded as the minimum activation energy (E_a) in kinetics. In principle, the overpotential is determined by the largest free energy increase (η = max[ΔG_1, ΔG_2, ΔG_3, ΔG_4]/e – 1.23 V) of the four steps. Ideally, in Fig. 8(a), the oxygen evolution catalyst should have a minimum overpotential (η = 0) when each of the four intermediates has the same free energy increase (1.23 eV) [73]. Thermodynamically, ideal electrocatalysts can meet this requirement; however, no real catalysts are expected for practical demonstrations of such a scenario.

Encouragingly, DFT calculations showed good agreement with experimental results on those state-of-the-art electrocatalysts. For example, Rossmeisl and Nørskov[71] investigated (110) surfaces of RuO_2 and IrO_2, where lower overpotentials were obtained due to the weak O binding but strong *OH binding on the surface. In a recent work on $Cr_5Ru_3O_{16}$ [75], the formation of *OOH was found to be the RDS with an energy barrier of 1.87 eV, which is smaller than that on RuO_2. For IrO_2[76], the highest energy barrier ($\Delta G_O - \Delta G_{OH}$ = 1.73 eV) on (110) surfaces is related to the conversion of *OH to form *O intermediates, corresponding to an overpotential of 0.5 V. As for lithium amorphous iridium oxide (Li-IrO_2), an overpotential of 0.4 V was calculated [76], which corresponded to the empty * intermediate formation.

The energy levels between intermediates display the bonding/interaction between the metal and oxygen. In previous work on $LaMO_3$ perovskite oxides, Man et al. found a linear relationship ($\Delta G_{OOH} - \Delta G_{OH}$ = 3.2 eV) between the *OOH and *OH intermediates [73]. Based on this linear relationship, a descriptor of $\Delta G_O - \Delta G_{OH}$ has been developed for catalyst optimization in the volcano plot (Fig. 8(b)). For example, when $\Delta G_O - \Delta G_{OH}$ > 1.6 eV for TiO_2, it indicates a weaker *O binding strength between the metal site and oxygen, so that it is easy to form an *OOH intermediate. When $\Delta G_O - \Delta G_{OH}$ < 1.6 eV, it indicates a stronger *O binding strength and *OOH formation as RDS. This scaling relationship has been applied in developing a new perovskite electrocatalyst [36, 77]. Generally, the main descriptor corresponding to the bonding strength between oxygen (or oxygenated intermediates) and the catalytic surface site, obeys the Sabatier principle: It is necessary to balance the interaction, neither too strong nor too weak [78].

This simple principle was successful in explaining an important observation: Fe_2O_3, TiO_2, WO_3, and $BiVO_4$ are not highly active electrocatalysts for water oxidation under dark conditions, even though they have been widely studied as efficient photocatalysts. The binding between the metal site and oxygen is much weaker than expected because the descriptor $\Delta G_O - \Delta G_{OH}$ is usually larger than 1.6 eV. For hematite, Hellman et al. found that the *O formation with an energy barrier of 2.09 eV was the RDS on (001) surfaces of the pristine oxygen-terminated crystal [79]. For anatase TiO_2, the *O formation was regarded as the RDS on (101) with an energy barrier at 2.62 eV [80]. For WO_3, the *O formation could be the RDS on (200), (020), and (002), with the energy barrier of 2.27–2.33 eV, respectively [72]. For $BiVO_4$, the RDS can be *O formation on (110) [81] and (011) [82] facets. It is worth noting that the DFT calculations are generally carried out on conventional WNA and I2M pathways on metal sites. It is also successful on other mechanisms, including LOM processes on perovskite oxides [33, 77] and Co-Zn oxyhydroxide [35].

For the purpose of decreasing the overpotentials of water oxidation on metal oxide surfaces, a number of approaches have been proposed to manipulate the energy barriers for various intermediates in the four-step reaction. For instance, Zhang et al. have found that the oxygen vacancy concentration is most effective in reducing the OER overpotential on hematite (110) surfaces [83], where a low overpotential of 0.47 V is predicted for 1.26 vacancies·nm^{-2}. A low overpotential of 0.52 V was found for the (100) surfaces with a bridge site configuration

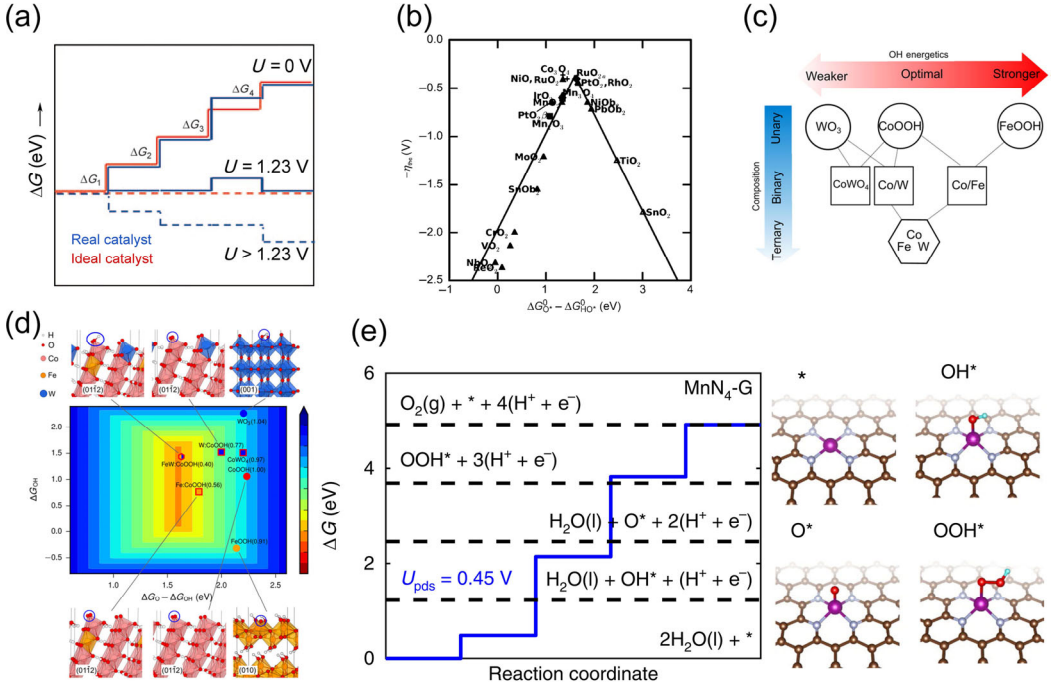

Figure 8 (a) Gibbs free energies for ideal (red) and actual (blue) catalysts. (b) Activity trends towards oxygen evolution in volcano plot with a descriptor of free energy of $\Delta G_{O^*} - \Delta G_{HO^*}$. (a) and (b) are adapted with permission from Ref. [73], © Wiley-VCH Verlag GmbH & Co. KGaA 2011. (c) Change in adsorption energetics (ΔG_{OH}) as a function of the increasing composition obtained by interpolation between calculated pure phases. (d) DFT+U calculated OER activities of pure and W-doped CoFe oxy-hydroxides and W oxides. (c) and (d) are reprinted with permission from Ref. [85], © American Association for the Advancement of Science 2016. (e) Free energy diagram for water oxidation on MnN_4-G by DFT simulations. Reprinted with permission from Ref. [86], © Guan, J. Q. et al. 2018.

that benefited from adsorbate-adsorbate interactions [84]. The metal–oxygen interaction of WO_3 is too weak, whereas the same interaction is too strong on FeOOH (Figs. 8(c) and 8(d)). Zhang et al. [85] fabricated FeCoW oxy-hydroxide with homogenous distribution of metal atoms, which demonstrated a low overpotential in alkaline electrolytes. The synergistic contribution between multiple W, Co, and Fe metals results in favorable local coordination environment and electronic structure which single metal cannot, making FeCoW be an excellent electrocatalyst. In Fig. 8(e), Li et al. [86] found that a heterogeneous catalyst with mononuclear manganese embedded in nitrogen-doped graphene (Mn-NG) exhibited a turnover frequency as high as 214 s^{-1} for water oxidation and a low overpotential of 337 mV at 10 $mA{\cdot}cm^{-2}$. DFT calculations showed an overpotential of 450 mV (*O formation as RDS) for MnN_4-G, which was much lower than that of trinuclear Mn_3N_7-G, or MnN_3-G or MnO_3-G, respectively. The water oxidation on the mononuclear Mn site is different from multinuclear complexes, and the RDS is the oxidation of *OH intermediate rather than the oxo-oxo coupling step.

DFT results can also shed light on the lowest (or negative) energy barrier/increment for the intermediates, which is powerful in predicting the initial intermediates. For example, under oxidation conditions, the Ru site could readily absorb OH to form *OH, as indicated by the lowest free energy barrier (0.51 eV for RuO_2 and 0.83 eV for $Cr_5Ru_3O_{16}$) [75]. Similarly, the *OH formation has the lowest energy barrier on IrO_2 [87]. However, the * formation from *OOH has the lowest energy barriers on some low-index facets of hematite [84], rutile (110) [72], anatase TiO_2 (001) [88], and $BiVO_4$ [89]. When the vacancies are introduced into the semiconductors (e.g., hematite), the energy barrier for *OH formation will be significantly reduced [90]. The calculations facilitate the discovering of high-performance electrocatalyst with the prediction of RDS and the overpotential. Although the reaction kinetics are suggested to be highly sensitive to the initial intermediates for the Tafel slope or rate-law studies, more studies are required to uncover this mystery. For instance, we recently showed that the oxidation mechanism could switch from IMOC at low overpotential to WNA process at high overpotential on cobalt-based water oxidation catalysts by altering the activity of water in the presence of water-in-salt electrolyte [54].

8 Summary and perspectives

The recent development of heterogeneous water oxidation catalysts has highlighted an intimate relationship between surface chemistry and the ultimate goal of achieving high-performance applications. In summarizing studies focused on this topic, we see the central role played by intermediate surface chemical species. Both experimental results and theoretical calculations confirm that some intermediates significantly influence the RDS and kinetics of the overall water oxidation reaction. The reaction is suggested to take place through a procedure similar to that in natural PS, in which multiple charges are accumulated at a catalytic cluster to overcome the RDS. Based on the summary we provided above, we suggest the following strategies to expedite research in this area.

(1) *In situ* and *operando* techniques: Only one or two intermediates are observed correlating with the applied bias or photon irradiation, which is proposed to be the active or RDS intermediates. Thus, it is not easy to substantiate a multiple-charge transfer reaction mechanism with a single method or intermediate. To validate these mechanisms, the intermediates at the electrocatalyst surface should be monitored by *in situ* or *operando* techniques [91]. The synchrotron-based X-ray absorption techniques [91–93], Raman spectroscopy [94–96], and infrared spectroscopy[97] for molecule/intermediate detection at the solid/electrolyte or solid/gas interface, just to name a few examples, will play increasingly more important roles.

(2) Theoretical calculations: Methods such as DFT, molecular dynamics, and machine learning have been developed to identify intermediates and transition states, which helps to predict the complex surface reactions with numerous reaction active sites, intermediates, and transition states. To bridge the understanding between experimental and theoretical advancements, more direct information such as the vibrational, adsorption, diffraction, and/or adsorption signals of the intermediates will be highly useful.

(3) Enable high charge densities on (photo)electrodes: For semiconducting materials, the charge density and potential drop would be more complex, as they are determined by the doping level, space charge capacitance, and the Helmholtz layer capacitance. However, the parameters (conductivity, flat band, and oxygen vacancy) only played a collective role in the OER activities[98]. By the use of the first-principle methods, Wang et al. suggested that the intrinsic OER catalytic activity of TiO_2 (110) under experimental conditions was not the rate-determining factor below the threshold [99]. The enhanced charge density at the electrocatalyst surface by structure designing can alter the reaction mechanisms.

(4) Catalyst with ideal energy barriers: An ideal catalyst requires all four steps to feature the same free energy increase (namely 1.23 eV at $U = 0$ V). Under this condition, the surface of the electrocatalyst would be uniformly covered by all possible intermediates. As the RDS is no longer valid, the water oxidation can be treated as a single-charge-transfer reaction. One can expect a Tafel slope of ~ 120 $mV{\cdot}dec^{-1}$ and a 1st-order reaction kinetics for the water oxidation. However, it seems to be an impossible situation to be achieved in practice: The adsorption energy of the intermediates such as *, *OH, *O, and *OOH, is not linearly correlated. Moreover, simple DFT calculations ignored the transition states, which should display higher activation energy than the free energy barrier, indicating the overpotential will be under-estimated through the intermediate level.

(5) Unique chemical environment and coordinates: The environments of the catalytic site could be furtherly modulated, which is a time-consuming process. First, the lattice vacancy involved OER can be intentionally designed from a single crystal, which can be well determined by fine X-ray analysis (like Natural PS). Second, the single-atom catalyst [100] with well-defined substrates can be regarded as a molecular catalyst, helping to shed light on the reaction mechanism. Third, some high-entropy metal compounds could be possible to alter the metal–oxygen bond [101]. The tunability of adsorption energies upon alloying would hence allow significant improvement in OER activity.

Acknowledgements

X. G. Y. and C. M. L. are supported by the National Natural Science Foundation of China (Nos. U1604121 and 22008163), Natural Science Foundation of Jiangsu Province (No. BK20180103), Jiangsu Laboratory for Biochemical Sensing and Biochip, and Jiangsu Key Laboratory for Micro and Nano Heat Fluid Flow Technology and Energy Application. Y. X. W. and D. W. W. acknowledge the support by the U.S. Department of Energy, Office of Science, Office of Basic Energy Science, Chemical

Sciences, Geosciences, and Biosciences Division under Award Number DE-SC0020261.

References

[1] Junge, W. Oxygenic photosynthesis: History, status and perspective. *Quart. Rev. Biophys*. **2019**, *52*, e1.

[2] Kornienko, N.; Zhang, J. Z.; Sakimoto, K. K.; Yang, P. D.; Reisner, E. Interfacing nature's catalytic machinery with synthetic materials for semi-artificial photosynthesis. *Nat. Nanotechnol*. **2018**, *13*, 890–899.

[3] Jia, J. Y.; Seitz, L. C.; Benck, J. D.; Huo, Y. J.; Chen, Y. S.; Ng, J. W. D.; Bilir, T.; Harris, J. S.; Jaramillo, T. F. Solar water splitting by photovoltaic-electrolysis with a solar-to-hydrogen efficiency over 30%. *Nat. Commun*. **2016**, *7*, 13237.

[4] Govind Rajan, A.; Martirez, J. M. P.; Carter, E. A. Why do we use the materials and operating conditions we use for heterogeneous (photo)electrochemical water splitting? *ACS Catal*. **2020**, *10*, 11177–11234.

[5] Yang, X. G.; Wang, D. W. Photocatalysis: From fundamental principles to materials and applications. *ACS Appl. Energy Mater*. **2018**, *1*, 6657–6693.

[6] Wang, C. H.; Li, C. M.; Liu, J. L.; Guo, C. X. Engineering transition metal-based nanomaterials for high-performance electrocatalysis. *Mater. Rep.: Energy* **2021**, *1*, 100006.

[7] Takashima, T.; Hashimoto, K.; Nakamura, R. Mechanisms of pH-dependent activity for water oxidation to molecular oxygen by MnO_2 electrocatalysts. *J. Am. Chem. Soc*. **2012**, *134*, 1519–1527.

[8] Chen, C.; Hu, J. D.; Yang, X. G.; Yang, T. Y.; Qu, J. F.; Guo, C. X.; Li, C. M. Ambient-stable black phosphorus-based 2D/2D S-scheme heterojunction for efficient photocatalytic CO_2 reduction to syngas. *ACS Appl. Mater. Interfaces* **2021**, *13*, 20162–20173.

[9] McCrory, C. C. L.; Jung, S.; Ferrer, I. M.; Chatman, S. M.; Peters, J. C.; Jaramillo, T. F. Benchmarking hydrogen evolving reaction and oxygen evolving reaction electrocatalysts for solar water splitting devices. *J. Am. Chem. Soc*. **2015**, *137*, 4347–4357.

[10] Lewis, N. S. Research opportunities to advance solar energy utilization. *Science* **2016**, *351*, aad1920.

[11] Mu, R. T.; Zhao, Z. J.; Dohnálek, Z.; Gong, J. L. Structural motifs of water on metal oxide surfaces. *Chem. Soc. Rev*. **2017**, *46*, 1785–1806.

[12] Xiao, Y.; Hu, T.; Zhao, X.; Hu, F. X.; Yang, H. B.; Li, C. M. Thermo-selenizing to rationally tune surface composition and evolve structure of stainless steel to electrocatalytically boost oxygen evolution reaction. *Nano Energy* **2020**, *75*, 104949.

[13] Li, J.; Triana, C. A.; Wan, W.; Adiyeri Saseendran, D. P.; Zhao, Y.; Balaghi, S. E.; Heidari, S.; Patzke, G. R. Molecular and heterogeneous water oxidation catalysts: Recent progress and joint perspectives. *Chem. Soc. Rev*. **2021**, *50*, 2444–2485.

[14] Wang, S. C.; Liu, G.; Wang, L. Z. Crystal facet engineering of photoelectrodes for photoelectrochemical water splitting. *Chem. Rev*. **2019**, *119*, 5192–5247.

[15] Seh, Z. W.; Kibsgaard, J.; Dickens, C. F.; Chorkendorff, I.; Nørskov, J. K.; Jaramillo, T. F. Combining theory and experiment in electrocatalysis: Insights into materials design. *Science* **2017**, *355*, eaad4998.

[16] Song, J. J.; Wei, C.; Huang, Z. F.; Liu, C. T.; Zeng, L.; Wang, X.; Xu, Z. J. A review on fundamentals for designing oxygen evolution electrocatalysts. *Chem. Soc. Rev*. **2020**, *49*, 2196–2214.

[17] Suen, N. T.; Hung, S. F.; Quan, Q.; Zhang, N.; Xu, Y. J.; Chen, H. M. Electrocatalysis for the oxygen evolution reaction: Recent development and future perspectives. *Chem. Soc. Rev*. **2017**, *46*, 337–365.

[18] Cox, N.; Pantazis, D. A.; Lubitz, W. Current understanding of the mechanism of water oxidation in photosystem ii and its relation to XFEL data. *Annu. Rev. Biochem*. **2020**, *89*, 795–820.

[19] Kern, J.; Chatterjee, R.; Young, I. D.; Fuller, F. D.; Lassalle, L.; Ibrahim, M.; Gul, S.; Fransson, T.; Brewster, A. S.; Alonso-Mori, R. et al. Structures of the intermediates of Kok's photosynthetic water oxidation clock. *Nature* **2018**, *563*, 421–425.

[20] Hunter, B. M.; Gray, H. B.; Müller, A. M. Earth-abundant heterogeneous water oxidation catalysts. *Chem. Rev*. **2016**, *116*, 14120–14136.

[21] Umena, Y.; Kawakami, K.; Shen, J. R.; Kamiya, N. Crystal structure of oxygen-evolving photosystem II at a resolution of 1.9 Å. *Nature* **2011**, *473*, 55–60.

[22] Kok, B.; Forbush, B.; McGloin, M. Cooperation of charges in photosynthetic O_2 evolution-I. A linear four step mechanism. *Photochem. Photobiol*. **1970**, *11*, 457–475.

[23] Zouni, A.; Witt, H. T.; Kern, J.; Fromme, P.; Krauss, N.; Saenger, W.; Orth, P. Crystal structure of photosystem II from *Synechococcus elongatus* at 3.8 Å resolution. *Nature* **2001**, *409*, 739–743.

[24] Haumann, M.; Liebisch, P.; Müller, C.; Barra, M.; Grabolle, M.; Dau, H. Photosynthetic O_2 formation tracked by time-resolved X-ray experiments. *Science* **2005**, *310*, 1019–1021.

[25] Zaharieva, I.; Wichmann, J. M.; Dau, H. Thermodynamic limitations of photosynthetic water oxidation at high proton concentrations. *J. Biol. Chem*. **2011**, *286*, 18222–18228.

[26] Ananyev, G.; Roy-Chowdhury, S.; Gates, C.; Fromme, P.; Dismukes, G. C. The catalytic cycle of water oxidation in crystallized photosystem ii complexes: Performance and requirements for formation of intermediates. *ACS Catal*. **2019**, *9*, 1396–1407.

[27] Armstrong, D. A.; Huie, R. E.; Koppenol, W. H.; Lymar, S. V.; Merényi, G.; Neta, P.; Ruscic, B.; Stanbury, D. M.; Steenken, S.; Wardman, P. Standard electrode potentials involving radicals in aqueous solution: Inorganic radicals (IUPAC Technical Report). *Pure Appl. Chem*. **2015**, *87*, 1139–1150.

[28] Hirakawa, T.; Yawata, K.; Nosaka, Y. Photocatalytic reactivity for O_2^{-} and OH· radical formation in anatase and rutile TiO_2 suspension as the effect of H_2O_2 addition. *Appl. Catal. A* **2007**, *325*, 105–111.

[29] Attri, P.; Kim, Y. H.; Park, D. H.; Park, J. H.; Hong, Y. J.; Uhm, H. S.; Kim, K. N.; Fridman, A.; Choi, E. H. Generation mechanism of hydroxyl radical species and its lifetime prediction during the plasma-initiated ultraviolet (UV) photolysis. *Sci. Rep*. **2015**, *5*, 9332.

[30] Craig, M. J.; Coulter, G.; Dolan, E.; Soriano-López, J.; Mates-Torres, E.; Schmitt, W.; García-Melchor, M. Universal scaling relations for the rational design of molecular water oxidation catalysts with near-zero overpotential. *Nat. Commun*. **2019**, *10*, 4993.

[31] Ullman, A. M.; Brodsky, C. N.; Li, N.; Zheng, S. L.; Nocera, D. G. Probing edge site reactivity of oxidic cobalt water oxidation catalysts. *J. Am. Chem. Soc*. **2016**, *138*, 4229–4236.

[32] Fabbri, E.; Schmidt, T. J. Oxygen evolution reaction—The enigma in water electrolysis. *ACS Catal*. **2018**, *8*, 9765–9774.

[33] Grimaud, A.; Diaz-Morales, O.; Han, B. H.; Hong, W. T.; Lee, Y. L.; Giordano, L.; Stoerzinger, K. A.; Koper, M. T. M.; Shao-Horn, Y. Activating lattice oxygen redox reactions in metal oxides to catalyse oxygen evolution. *Nat. Chem*. **2017**, *9*, 457–465.

[34] Geiger, S.; Kasian, O.; Ledendecker, M.; Pizzutilo, E.; Mingers, A. M.; Fu, W. T.; Diaz-Morales, O.; Li, Z. Z.; Oellers, T.; Fruchter, L. et al. The stability number as a metric for electrocatalyst stability benchmarking. *Nat. Catal*. **2018**, *1*, 508–515.

[35] Huang, Z. F.; Song, J. J.; Du, Y. H.; Xi, S. B.; Dou, S.; Nsanzimana, J. M. V.; Wang, C.; Xu, Z. J.; Wang, X. Chemical and structural origin of lattice oxygen oxidation in Co–Zn oxyhydroxide oxygen evolution electrocatalysts. *Nat. Energy* **2019**, *4*, 329–338.

[36] Pan, Y. L.; Xu, X. M.; Zhong, Y. J.; Ge, L.; Chen, Y. B.; Veder, J. P. M.; Guan, D. Q.; O'Hayre, R.; Li, M. R.; Wang, G. X. et al. Direct evidence of boosted oxygen evolution over perovskite by enhanced lattice oxygen participation. *Nat. Commun*. **2020**, *11*, 2002.

[37] Mondal, S.; Mohanty, B.; Nurhuda, M.; Dalapati, S.; Jana, R.; Addicoat, M.; Datta, A.; Jena, B. K.; Bhaumik, A. A thiadiazole-based covalent organic framework: A metal-free electrocatalyst toward oxygen evolution reaction. *ACS Catal*. **2020**, *10*, 5623–5630.

[38] Lee, C. H.; Jun, B.; Lee, S. U. Metal-free oxygen evolution and oxygen reduction reaction bifunctional electrocatalyst in alkaline media: From mechanisms to structure–catalytic activity relationship. *ACS Sustain. Chem. Eng*. **2018**, *6*, 4973–4980.

[39] Zhang, Y. C.; Zhang, H. N.; Liu, A. A.; Chen, C. C.; Song, W. J.; Zhao, J. C. Rate-limiting O–O bond formation pathways for water oxidation on hematite photoanode. *J. Am. Chem. Soc*. **2018**, *140*, 3264–3269.

[40] Zhang, M.; Frei, H. Water oxidation mechanisms of metal oxide catalysts by vibrational spectroscopy of transient intermediates. *Annu. Rev. Phys. Chem*. **2017**, *68*, 209–231.

[41] Makoto, E.; Shohachi, K.; Shuichi, K.; Tetsuro, S. Temperature programmed desorption study of water adsorbed on metal oxides. I. Anatase and rutile. *Bull. Chem. Soc. Jpn*. **1978**, *51*, 3144–3149.

[42] Lindan, P. J. D.; Harrison, N. M.; Gillan, M. J. Mixed dissociative and molecular adsorption of water on the rutile (110) surface. *Phys. Rev. Lett.* **1998**, *80*, 762–765.

[43] Vittadini, A.; Selloni, A.; Rotzinger, F. P.; Grätzel, M. Structure and energetics of water adsorbed at TiO_2 anatase (101) and (001) surfaces. *Phys. Rev. Lett.* **1998**, *81*, 2954–2957.

[44] Yamamoto, S.; Kendelewicz, T.; Newberg, J. T.; Ketteler, G.; Starr, D. E.; Mysak, E. R.; Andersson, K. J.; Ogasawara, H.; Bluhm, H.; Salmeron, M. et al. Water adsorption on α-Fe_2O_3 (0001) at near ambient conditions. *J. Phys. Chem. C* **2010**, *114*, 2256–2266.

[45] Albanese, E.; Di Valentin, C.; Pacchioni, G. H_2O adsorption on WO_3 and WO_{3-x} (001) surfaces. *ACS Appl. Mater. Interfaces* **2017**, *9*, 23212–23221.

[46] Zhang, L.; Wen, B.; Zhu, Y. N.; Chai, Z. W.; Chen, X. G.; Chen, M. Y. First-principles calculations of water adsorption on perfect and defect WO_3 (001). *Comput. Mater. Sci.* **2018**, *150*, 484–490.

[47] Oshikiri, M.; Boero, M. Water molecule adsorption properties on the $BiVO_4$ (100) surface. *J. Phys. Chem. B* **2006**, *110*, 9188–9194.

[48] Li, P.; Chen, X. Y.; He, H. C.; Zhou, X.; Zhou, Y.; Zou, Z. G. Polyhedral 30-faceted $BiVO_4$ microcrystals predominantly enclosed by high-index planes promoting photocatalytic water-splitting activity. *Adv. Mater.* **2018**, *30*, 1703119.

[49] Hurtado-Aular, O.; Vidal, A. B.; Sierraalta, A.; Añez, R. Periodic DFT study of water adsorption on m-WO_3(001), m-WO_3(100), h-WO_3(001) and h-WO_3(100). Role of hydroxyl groups on the stability of polar hexagonal surfaces. *Surf. Sci.* **2020**, *694*, 121558.

[50] Sivasankar, N.; Weare, W. W.; Frei, H. Direct observation of a hydroperoxide surface intermediate upon visible light-driven water oxidation at an Ir oxide nanocluster catalyst by rapid-scan FT-IR spectroscopy. *J. Am. Chem. Soc.* **2011**, *133*, 12976–12979.

[51] Zhang, M.; de Respinis, M.; Frei, H. Time-resolved observations of water oxidation intermediates on a cobalt oxide nanoparticle catalyst. *Nat. Chem.* **2014**, *6*, 362–367.

[52] Zandi, O.; Hamann, T. W. Determination of photoelectrochemical water oxidation intermediates on haematite electrode surfaces using operando infrared spectroscopy. *Nat. Chem.* **2016**, *8*, 778–783.

[53] Diaz-Morales, O.; Ferrus-Suspedra, D.; Koper, M. T. M. The importance of nickel oxyhydroxide deprotonation on its activity towards electrochemical water oxidation. *Chem. Sci.* **2016**, *7*, 2639–2645.

[54] Lang, C. C.; Li, J. Y.; Yang, K. R.; Wang, Y. X.; He, D.; Thorne, J. E.; Croslow, S.; Dong, Q.; Zhao, Y. Y.; Prostko, G. et al. Observation of a potential-dependent switch of water-oxidation mechanism on Co-oxide-based catalysts. *Chem,* in press, DOI: 10.1016/j.chempr.2021.03.015.

[55] Barroso, M.; Pendlebury, S. R.; Cowan, A. J.; Durrant, J. R. Charge carrier trapping, recombination and transfer in hematite (α-Fe_2O_3) water splitting photoanodes. *Chem. Sci.* **2013**, *4*, 2724–2734.

[56] Kafizas, A.; Ma, Y. M.; Pastor, E.; Pendlebury, S. R.; Mesa, C.; Francàs, L.; Le Formal, F.; Noor, N.; Ling, M.; Sotelo-Vazquez, C. et al. Water oxidation kinetics of accumulated holes on the surface of a TiO_2 photoanode: A rate law analysis. *ACS Catal.* **2017**, *7*, 4896–4903.

[57] Shinagawa, T.; Garcia-Esparza, A. T.; Takanabe, K. Insight on Tafel slopes from a microkinetic analysis of aqueous electrocatalysis for energy conversion. *Sci. Rep.* **2015**, *5*, 13801.

[58] Fang, Y. H.; Liu, Z. P. Tafel kinetics of electrocatalytic reactions: From experiment to first-principles. *ACS Catal.* **2014**, *4*, 4364–4376.

[59] Zhang, J. M.; Tao, H. B.; Kuang, M.; Yang, H. B.; Cai, W. Z.; Yan, Q. Y.; Mao, Q.; Liu, B. Advances in thermodynamic-kinetic model for analyzing the oxygen evolution reaction. *ACS Catal.* **2020**, *10*, 8597–8610.

[60] Nong, H. N.; Falling, L. J.; Bergmann, A.; Klingenhof, M.; Tran, H. P.; Spöri, C.; Mom, R.; Timoshenko, J.; Zichittella, G.; Knop-Gericke, A. et al. Key role of chemistry versus bias in electrocatalytic oxygen evolution. *Nature* **2020**, *587*, 408–413.

[61] Peter, L. Kinetics and mechanisms of light-driven reactions at semiconductor electrodes: Principles and techniques. In *Photo-electrochemical Water Splitting: Materials, Processes and Architectures*; Lewerenz, H. J.; Peter, L., Eds.; The Royal Society of Chemistry: Cambridge, 2013; pp 19–51.

[62] Le Formal, F.; Pastor, E.; Tilley, S. D.; Mesa, C. A.; Pendlebury, S. R.; Grätzel, M.; Durrant, J. R. Rate law analysis of water oxidation on a hematite surface. *J. Am. Chem. Soc.* **2015**, *137*, 6629–6637.

[63] Ma, Y. M.; Mesa, C. A.; Pastor, E.; Kafizas, A.; Francàs, L.; Le Formal, F.; Pendlebury, S. R.; Durrant, J. R. Rate law analysis of water oxidation and hole scavenging on a $BiVO_4$ photoanode. *ACS Energy Lett.* **2016**, *1*, 618–623.

[64] Mesa, C. A.; Francàs, L.; Yang, K. R.; Garrido-Barros, P.; Pastor, E.; Ma, Y. M.; Kafizas, A.; Rosser, T. E.; Mayer, M. T.; Reisner, E. et al. Multihole water oxidation catalysis on haematite photoanodes revealed by operando spectroelectrochemistry and DFT. *Nat. Chem.* **2020**, *12*, 82–89.

[65] Li, J. G.; Wan, W. C.; Triana, C. A.; Chen, H.; Zhao, Y. G.; Mavrokefalos, C. K.; Patzke, G. R. Reaction kinetics and interplay of two different surface states on hematite photoanodes for water oxidation. *Nat. Commun.* **2021**, *12*, 255.

[66] Li, J. G.; Wan, W. C.; Triana, C. A.; Novotny, Z.; Osterwalder, J.; Erni, R.; Patzke, G. R. Dynamic role of cluster cocatalysts on molecular photoanodes for water oxidation. *J. Am. Chem. Soc.* **2019**, *141*, 12839–12848.

[67] Zhang, Z. J.; Nagashima, H.; Tachikawa, T. Ultra-narrow depletion layers in a hematite mesocrystal-based photoanode for boosting multihole water oxidation. *Angew. Chem., Int. Ed.* **2020**, *59*, 9047–9054.

[68] Francàs, L.; Corby, S.; Selim, S.; Lee, D.; Mesa, C. A.; Godin, R.; Pastor, E.; Stephens, I. E. L.; Choi, K. S.; Durrant, J. R. Spectroelectrochemical study of water oxidation on nickel and iron oxyhydroxide electrocatalysts. *Nat. Commun.* **2019**, *10*, 5208.

[69] Nørskov, J. K.; Bligaard, T.; Rossmeisl, J.; Christensen, C. H. Towards the computational design of solid catalysts. *Nat. Chem.* **2009**, *1*, 37–46.

[70] Montoya, J. H.; Seitz, L. C.; Chakthranont, P.; Vojvodic, A.; Jaramillo, T. F.; Norskov, J. K. Materials for solar fuels and chemicals. *Nat. Mater.* **2017**, *16*, 70–81.

[71] Rossmeisl, J.; Qu, Z. W.; Zhu, H.; Kroes, G. J.; Nørskov, J. K. Electrolysis of water on oxide surfaces. *J. Electroanal. Chem.* **2007**, *607*, 83–89.

[72] Valdés, Á.; Qu, Z. W.; Kroes, G. J.; Rossmeisl, J.; Nørskov, J. K. Oxidation and photo-oxidation of water on TiO_2 surface. *J. Phys. Chem. C* **2008**, *112*, 9872–9879.

[73] Man, I. C.; Su, H. Y.; Calle-Vallejo, F.; Hansen, H. A.; Martínez, J. I.; Inoglu, N. G.; Kitchin, J.; Jaramillo, T. F.; Nørskov, J. K.; Rossmeisl, J. Universality in oxygen evolution electrocatalysis on oxide surfaces. *ChemCatChem* **2011**, *3*, 1159–1165.

[74] Bajdich, M.; García-Mota, M.; Vojvodic, A.; Nørskov, J. K.; Bell, A. T. Theoretical investigation of the activity of cobalt oxides for the electrochemical oxidation of water. *J. Am. Chem. Soc.* **2013**, *135*, 13521–13530.

[75] Lin, Y. C.; Tian, Z. Q.; Zhang, L. J.; Ma, J. Y.; Jiang, Z.; Deibert, B. J.; Ge, R. X.; Chen, L. Chromium-ruthenium oxide solid solution electrocatalyst for highly efficient oxygen evolution reaction in acidic media. *Nat. Commun.* **2019**, *10*, 162.

[76] Gao, J. J.; Xu, C. Q.; Hung, S. F.; Liu, W.; Cai, W. Z.; Zeng, Z. P.; Jia, C. M.; Chen, H. M.; Xiao, H.; Li, J. et al. Breaking long-range order in iridium oxide by alkali ion for efficient water oxidation. *J. Am. Chem. Soc.* **2019**, *141*, 3014–3023.

[77] Hwang, J.; Rao, R. R.; Giordano, L.; Katayama, Y.; Yu, Y.; Shao-Horn, Y. Perovskites in catalysis and electrocatalysis. *Science* **2017**, *358*, 751–756.

[78] Dau, H.; Limberg, C.; Reier, T.; Risch, M.; Roggan, S.; Strasser, P. The mechanism of water oxidation: From electrolysis via homogeneous to biological catalysis. *ChemCatChem* **2010**, *2*, 724–761.

[79] Hellman, A.; Iandolo, B.; Wickman, B.; Grönbeck, H.; Baltrusaitis, J. Electro-oxidation of water on hematite: Effects of surface termination and oxygen vacancies investigated by first-principles. *Surf. Sci.* **2015**, *640*, 45–49.

[80] Li, Y. F.; Liu, Z. P.; Liu, L. L.; Gao, W. G. Mechanism and activity of photocatalytic oxygen evolution on titania anatase in aqueous surroundings. *J. Am. Chem. Soc.* **2010**, *132*, 13008–13015.

[81] Hu, J.; Chen, W.; Zhao, X.; Su, H. B.; Chen, Z. Anisotropic electronic characteristics, adsorption, and stability of low-index $BiVO_4$ surfaces for photoelectrochemical applications. *ACS Appl. Mater. Interfaces* **2018**, *10*, 5475–5484.

[82] Yang, J. X.; Wang, D. E.; Zhou, X.; Li, C. A theoretical study on the mechanism of photocatalytic oxygen evolution on $BiVO_4$ in aqueous solution. *Chem.—Eur. J.* **2013**, *19*, 1320–1326.
[83] Zhang, X. Q.; Klaver, P.; van Santen, R.; van de Sanden, M. C. M.; Bieberle-Hütter, A. Oxygen evolution at hematite surfaces: The impact of structure and oxygen vacancies on lowering the overpotential. *J. Phys. Chem. C* **2016**, *120*, 18201–18208.
[84] Zhang, X. Q.; Cao, C. L.; Bieberle-Hütter, A. Orientation sensitivity of oxygen evolution reaction on hematite. *J. Phys. Chem. C* **2016**, *120*, 28694–28700.
[85] Zhang, B.; Zheng, X. L.; Voznyy, O.; Comin, R.; Bajdich, M.; García-Melchor, M.; Han, L. L.; Xu, J. X.; Liu, M.; Zheng, L. R. et al. Homogeneously dispersed multimetal oxygen-evolving catalysts. *Science* **2016**, *352*, 333–337.
[86] Guan, J. Q.; Duan, Z. Y.; Zhang, F. X.; Kelly, S. D.; Si, R.; Dupuis, M.; Huang, Q. E.; Chen, J. Q.; Tang, C. H.; Li, C. Water oxidation on a mononuclear manganese heterogeneous catalyst. *Nat. Catal.* **2018**, *1*, 870–877.
[87] Gauthier, J. A.; Dickens, C. F.; Chen, L. D.; Doyle, A. D.; Nørskov, J. K. Solvation effects for oxygen evolution reaction catalysis on IrO_2(110). *J. Phys. Chem. C* **2017**, *121*, 11455–11463.
[88] Kenmoe, S.; Spohr, E. Photooxidation of water on pristine, S- and N-doped TiO_2(001) nanotube surfaces: A DFT + *U* study. *J. Phys. Chem. C* **2019**, *123*, 22691–22698.
[89] Yang, M. J.; He, H. C.; Liao, A. Z.; Huang, J.; Tang, Y.; Wang, J.; Ke, G. L.; Dong, F. Q.; Yang, L.; Bian, L. et al. Boosted water oxidation activity and kinetics on $BiVO_4$ photoanodes with multihigh-index crystal facets. *Inorg. Chem.* **2018**, *57*, 15280–15288.
[90] Nguyen, M. T.; Piccinin, S.; Seriani, N.; Gebauer, R. Photo-oxidation of water on defective hematite(0001). *ACS Catal.* **2015**, *5*, 715–721.
[91] Li, X. N.; Wang, H. Y.; Yang, H. B.; Cai, W. Z.; Liu, S.; Liu, B. *In situ*/operando characterization techniques to probe the electrochemical reactions for energy conversion. *Small Methods* **2018**, *2*, 1700395.
[92] Deng, J. J.; Zhang, Q. Z.; Lv, X. X.; Zhang, D.; Xu, H.; Ma, D. L.; Zhong, J. Understanding photoelectrochemical water oxidation with X-ray absorption spectroscopy. *ACS Energy Lett.* **2020**, *5*, 975–993.
[93] Timoshenko, J.; Roldan Cuenya, B. *In situ*/*operando* electrocatalyst characterization by X-ray absorption spectroscopy. *Chem. Rev.* **2021**, *121*, 882–961.
[94] Joya, K. S.; Sala, X. *In situ* Raman and surface-enhanced Raman spectroscopy on working electrodes: Spectroelectrochemical characterization of water oxidation electrocatalysts. *Phys. Chem. Chem. Phys.* **2015**, *17*, 21094–21103.
[95] Deng, Y. L.; Yeo, B. S. Characterization of electrocatalytic water splitting and CO_2 reduction reactions using *in situ*/operando Raman spectroscopy. *ACS Catal.* **2017**, *7*, 7873–7889.
[96] Qiu, Z.; Ma, Y.; Edvinsson, T. *In operando* Raman investigation of Fe doping influence on catalytic NiO intermediates for enhanced overall water splitting. *Nano Energy* **2019**, *66*, 104118.
[97] Rao, R. R.; Kolb, M. J.; Giordano, L.; Pedersen, A. F.; Katayama, Y.; Hwang, J.; Mehta, A.; You, H.; Lunger, J. R.; Zhou, H. et al. Operando identification of site-dependent water oxidation activity on ruthenium dioxide single-crystal surfaces. *Nat. Catal.* **2020**, *3*, 516–525.
[98] Cheng, X.; Fabbri, E.; Yamashita, Y.; Castelli, I. E.; Kim, B.; Uchida, M.; Haumont, R.; Puente-Orench, I.; Schmidt, T. J. Oxygen evolution reaction on perovskites: A multieffect descriptor study combining experimental and theoretical methods. *ACS Catal.* **2018**, *8*, 9567–9578.
[99] Wang, D.; Sheng, T.; Chen, J. F.; Wang, H. F.; Hu, P. Identifying the key obstacle in photocatalytic oxygen evolution on rutile TiO_2. *Nat. Catal.* **2018**, *1*, 291–299.
[100] Cao, L. L.; Luo, Q. Q.; Chen, J. J.; Wang, L.; Lin, Y.; Wang, H. J.; Liu, X. K.; Shen, X. Y.; Zhang, W.; Liu, W. et al. Dynamic oxygen adsorption on single-atomic ruthenium catalyst with high performance for acidic oxygen evolution reaction. *Nat. Commun.* **2019**, *10*, 4849.
[101] Ma, P. Y.; Zhang, S. C.; Zhang, M. T.; Gu, J. F.; Zhang, L.; Sun, Y. C.; Ji, W.; Fu, Z. Y. Hydroxylated high-entropy alloy as highly efficient catalyst for electrochemical oxygen evolution reaction. *Sci. China Mater.* **2020**, *63*, 2613–2619.